Appendix A

Profile Migration by the Hybrid Method

In this Appendix, I compare profile migration by double downward continuation with profile migration using the hybrid method. In the hybrid method, the downward continuation of the source is replaced by time shifting. For this comparison, I assume a constant velocity; the arguments can be easily extended to media in which ray theory applies.

A.1 PROFILE MIGRATION BY DOUBLE DOWNWARD CONTINUATION

The reflectivity of the subsurface, R, can be estimated by the ratio between the upgoing field, U, and the downgoing field, D, (Clærbout, 1985). For a given frequency, ω,

$$
\begin{aligned}
R(x, z, \omega) &= \frac{U(x, z, \omega)}{D(x, z, \omega)} \\
&= \frac{U(x, z, \omega) D^*(x, z, \omega)}{D(x, z, \omega) D^*(x, z, \omega)} \\
&= \frac{U(x, z, \omega) D^*(x, z, \omega)}{|D(x, z, \omega)|^2} \, ,
\end{aligned}
\tag{A.1}
$$

where * denotes conjugation. UD^* is the cross-correlation between the upgoing and downgoing fields in the frequency domain; integration over ω gives the zero-lag cross-correlation. At a given frequency, the denominator in (A.1) is a wave divergence correction that depends on x and z. Because of the instability of dividing by $|D|^2$, this factor is either ignored or damped by the addition of a constant.

In equation (A.1) it is assumed that there is no variation in the y direction. The source and receivers are, therefore, cylindrical (line source and receivers). The Green's function

for a line source is

$$G(k_x, z, \omega) = \frac{e^{-ik_z z}}{ik_z} ,$$

where $k_z = \sqrt{\frac{\omega^2}{v^2} - k_x^2}$. The division by k_z implies a cosine weighting with ray angle. This weighting is ignored in zero-offset migration because each receiver is assumed to be associated with its own source in the exploding-reflector model, which makes the cosine factor to be equal to 1.

To obtain the migrated image, we first extrapolate the field recorded at the surface, $p(x, z = 0, t)$, to the depth z. As in post-stack migration, extrapolation can be done by applying a phase shift in the frequency-wavenumber domain when the velocity does not vary laterally,

$$p(k_x, z, \omega) = p(k_x, 0, \omega)e^{-iz\sqrt{\frac{\omega^2}{v^2} - k_x^2}} . \tag{A.2}$$

When the velocity varies laterally, finite differencing can be used.

Because imaging is done in the space domain, we need to Fourier transform equation (A.2),

$$p(x, z, \omega) = \int p(k_x, 0, \omega)e^{-iz\sqrt{\frac{\omega^2}{v^2} - k_x^2}}e^{-ik_x x}dk_x . \tag{A.3}$$

Next, we extrapolate the source and apply the imaging principle in (A.1) to obtain the reflectivity at a given frequency. The migrated image (at $t = 0$) is obtained by adding all frequencies,

$$p_1(x, z, t = 0) =$$

$$\int \left[\int p(k_x, 0, \omega)e^{-iz\sqrt{\frac{\omega^2}{v^2} - k_x^2}}e^{-ik_x x}dk_x \right] \left[\int \frac{e^{-iz\sqrt{\frac{\omega^2}{v^2} - k_x^2}}}{i\sqrt{\frac{\omega^2}{v^2} - k_x^2}}e^{-ik_x x}dk_x \right]^* |D(x, z, \omega)|^{-2} d\omega . \tag{A.4}$$

The limits of the integrals in equation (A.4) and all other integrals in this appendix are from $-\infty$ to ∞.

A.2 PROFILE MIGRATION BY THE HYBRID METHOD

Because a profile has only one source, it is easy to compute the source extrapolation term analytically by ray tracing, which is cheaper than downward continuation. This (hybrid) method therefore mixes wave-theoretical extrapolation of the receiver wavefield with ray-theoretical time shifting of the source wavefield. The amount of the time shift for a receiver is equal to the traveltime from the source to that receiver at the new depth and can be determined by ray tracing. The image at $t = 0$ is then mapped to the output at that depth. The method was used by Al-Yahya and Muir (1984) and by Reshef and Kosloff (1986). This method is schematically shown in Figure A.1. Note that while the downward continuation paths are normal, the energy also moves laterally besides moving downward as the receivers are downward continued. The result is that the illuminated area is limited to half the cable length for a flat reflector.

Replacing the downward continuation by time shifting assumes that ray theory can be used. Ray theory breaks down if the medium has properties that change within a distance that is less than the wavelength of the propagating wave.
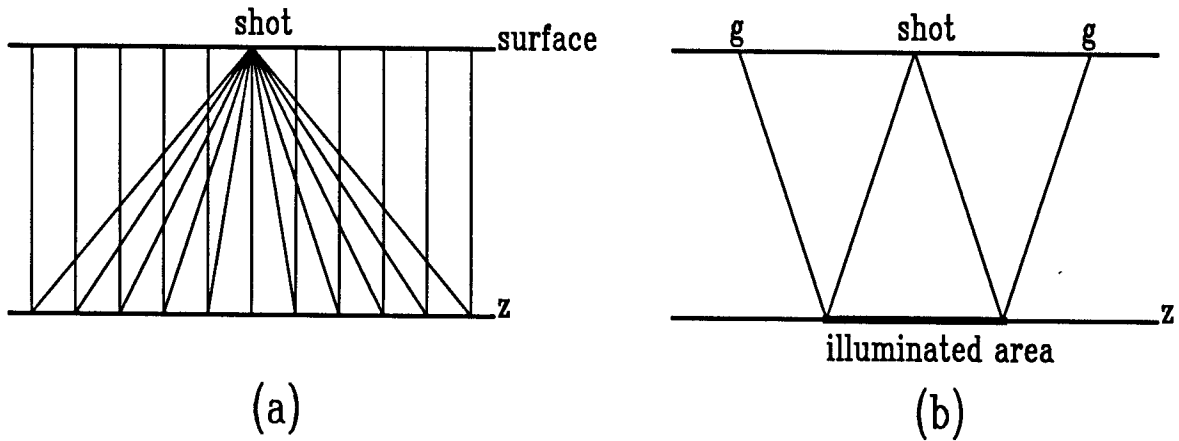

FIG. A.1. (a) A schematic diagram of profile migration by the hybrid method. Vertical lines are the downward continuation paths and slanted lines are the time shifting paths. Note that while the downward continuation paths are normal, the energy also moves laterally as the receivers are continued. The result is that the illuminated area is shorter than the cable length as shown in (b).

The imaging principle used for this method is similar to the one used in post-stack migration. In post-stack migration, where the exploding reflector model is used, the image

is taken to be at $t = 0$ after extrapolation. In profile migration, the image is taken to be at $t = \tau$, where τ is the traveltime from the source to the receiver at that depth. Alternatively, we can shift the extrapolated field by τ and take the image at $t = 0$. For a constant-velocity model, $\tau = \sqrt{x^2 + z^2}/v$ and the migrated gather is

$$
\begin{aligned}
p_2(x, z, t = 0) &= \int \left[\int p(k_x, 0, \omega) e^{-iz\sqrt{\frac{\omega^2}{v^2} - k_x^2}} e^{-ik_x x} dk_x \right] e^{+i\frac{\omega}{v}\sqrt{x^2 + z^2}} \sqrt{x^2 + z^2} \, d\omega \\
&= \int \left[\int p(k_x, 0, \omega) e^{-iz\sqrt{\frac{\omega^2}{v^2} - k_x^2}} e^{-ik_x x} dk_x \right] \left[\frac{e^{-i\frac{\omega}{v}\sqrt{x^2 + z^2}}}{\sqrt{x^2 + z^2}} \right]^{-1} d\omega \ , \quad (A.5)
\end{aligned}
$$

where a divergence correction is also applied by multiplying by $\sqrt{x^2 + z^2}$.

Note that in both (A.4) and (A.5), the extrapolation of the upgoing waves is done in the same way, so line receivers are assumed in both cases. The difference between the two equations lies in the source-extrapolation terms. In equation (A.4), a line source was assumed while in equation (A.5) a point source at $y = 0$ is assumed.

A.3 GREEN'S FUNCTIONS

The last term in the integrand of (A.5) is nothing but the reciprocal of the Green's function of a point source. Figure A.2 compares it to the conjugate of the Green's function of a line source in (A.4) for a given depth and frequency. The figure shows that there is both an amplitude and a phase difference between the two functions.

To explain the differences that appear in Figure A.2, I will compare the two Green's functions in the space domain. The Green's function for a line source is the Hankel function of zero order. This is easily obtained by noting that the general solution of the wave equation in cylindrical coordinates is a linear combination of the zero-order Hankel functions of the first and second kind,

$$
G(r, \omega) = c_1 H_0^{(1)}(\frac{\omega}{v}r) + c_2 H_0^{(2)}(\frac{\omega}{v}r) \ ,
$$

where c_1 and c_2 are constants (for a given frequency); $H_0^{(1)}(.)$ represents the outward traveling wave while $H_0^{(2)}(.)$ represents the inward traveling wave. If we have a line source,
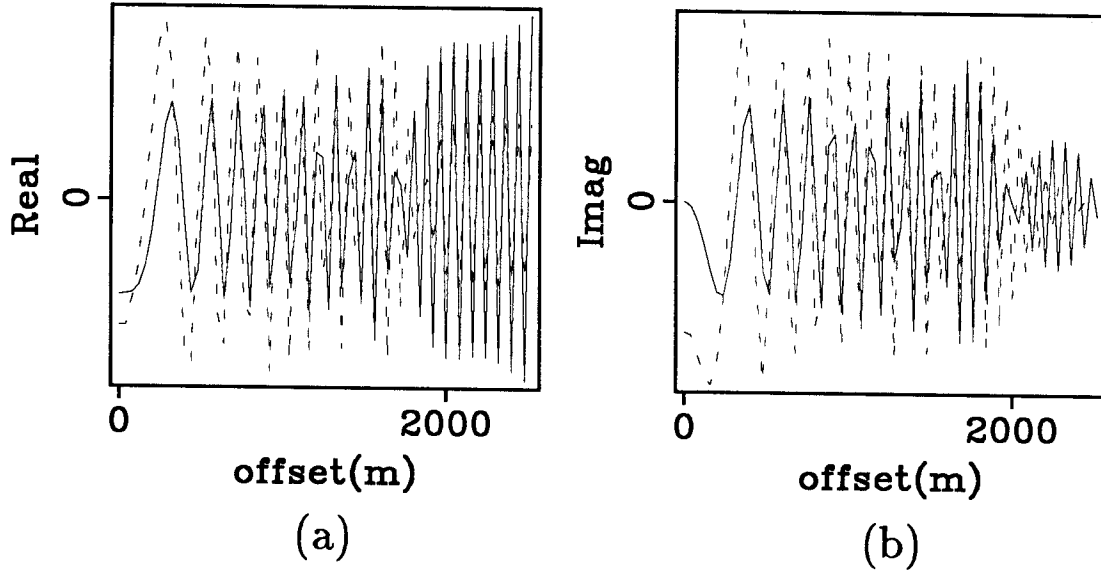
FIG. A.2. The source-extrapolation terms at a given depth and frequency. The solid line is for a point source; the dashed line is for a line source. (a) Real part. (b) Imaginary part. Parameters are: frequency=45 Hz, v=3 km/sec, dx=40 m, z=1.5 km. Both functions have been normalized to get rid of multiplicative constants.

then there is only an outward traveling wave. Therefore,

$$G(x,z,\omega) = c_1 H_0^{(1)}(\frac{\omega}{v}\sqrt{x^2 + z^2}) \ . \tag{A.6}$$

For large arguments, the Hankel function has the asymptotic expansion

$$H_0^{(1)}(a) \approx \sqrt{\frac{2}{\pi a}} \, e^{-i(a-\frac{\pi}{4})} \ ,$$

Abramowitz and Stegun (1965) (for small arguments it has a logarithmic singularity). Therefore, for large arguments, the Green's function for a line source is

$$G(x,z,\omega) \sim \sqrt{\frac{v}{\omega\sqrt{x^2+z^2}}} \, e^{-i(\frac{\omega}{v}\sqrt{x^2+z^2}-\frac{\pi}{4})} \ , \tag{A.7}$$

which I will take to represent D in (A.4). The large argument requirement in (A.7) means it is valid for the far field or high frequency, namely when ray theory applies.

The first difference between (A.4) and (A.5) is the $\pi/4$ phase shift that is found in (A.7). This phase shift is clearly observed in Figure A.2. The second difference between (A.4) and (A.5) is the divergence correction. In (A.5), the divergence correction is $\sqrt{x^2 + z^2}$. To obtain the divergence correction in (A.4), we need to compute $|D|^{-2}$. From (A.7),

$$|D(x,z,\omega)|^{-2} \sim \omega (x^2 + z^2)^{\frac{1}{2}}$$

$$= \omega\, div(x,z)\ , \tag{A.8}$$

where $div(x,z)$ is a divergence correction. Note that it is the same as the divergence correction in (A.5). Allowing for the $\pi/4$ phase shift and the divergence correction, we see in Figure A.3 that the amplitudes and phase become much more similar. It is important, however, to note that the figures shown correspond to *one* frequency. When adding the various frequency components using equation (A.4), observe that the terms are ω-dependent. This dependence comes from two places, ω in (A.8) and the coefficient a in (A.6) (which is ω-dependent).
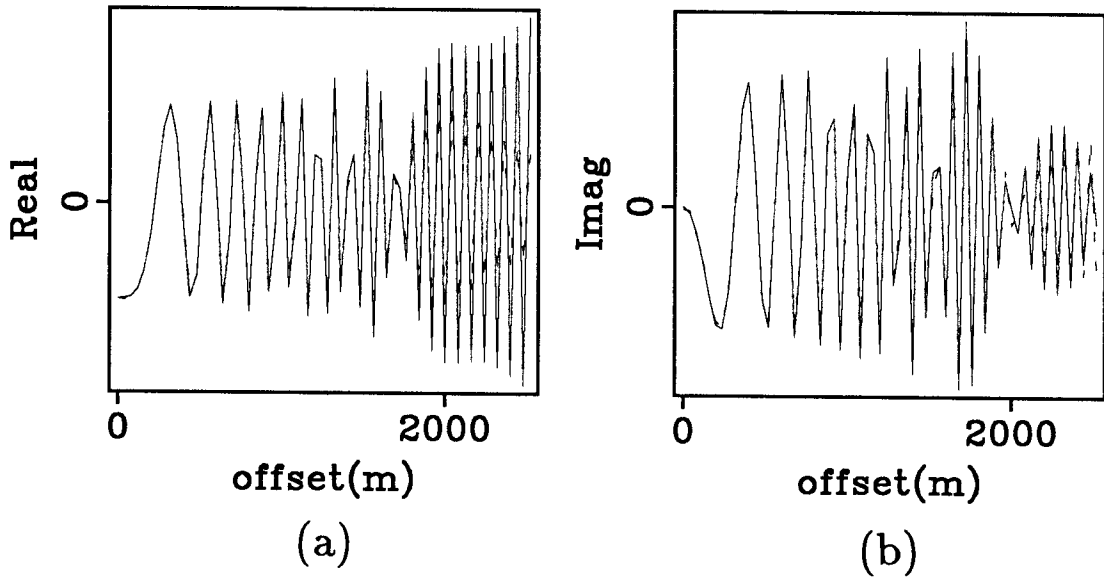

FIG. A.3. The result of applying divergence correction and a $\pi/4$ phase shift to the dashed line in Figure A.2. The functions were scaled so that they match at small offsets. (a) The real part. (b) The imaginary part.

offset(km)

-1   0

time(sec)

0

1

2

(a)
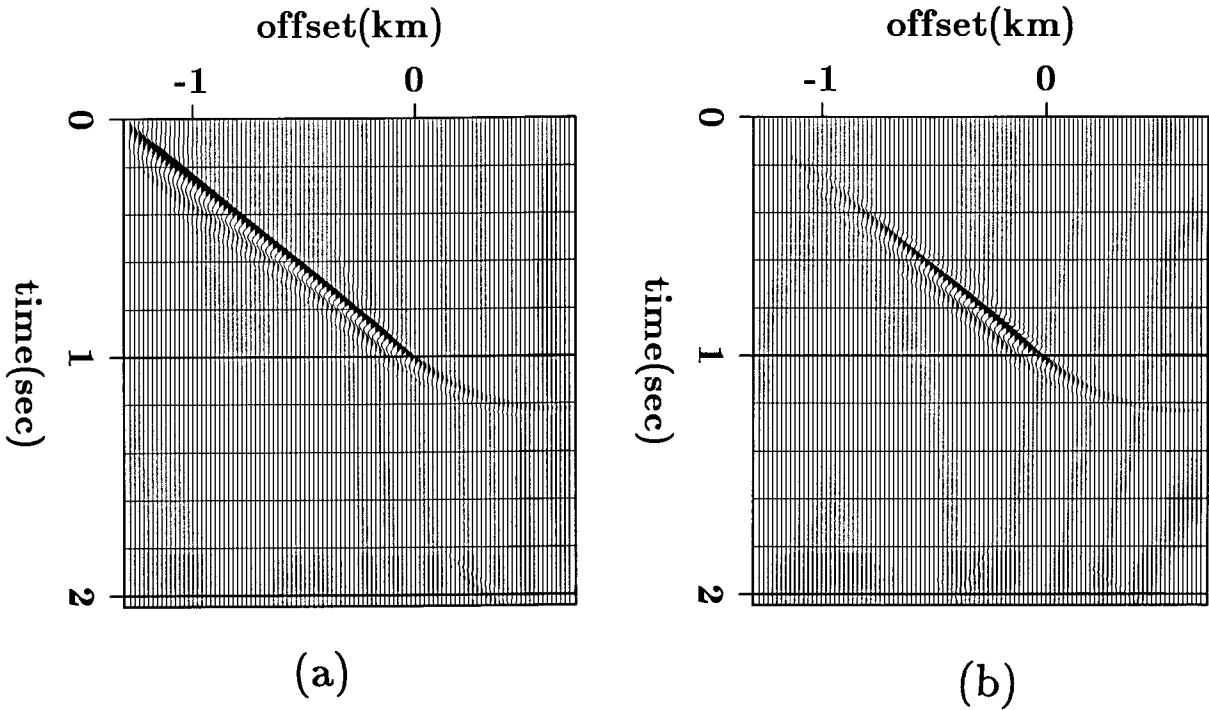
offset(km)

-1   0

time(sec)

0

1

2

(b)

FIG. A.4. A migrated dipping reflector. (a) by downward continuation of receivers and time-shifting. (b) by downward continuation of both source and receivers and cross-correlating.
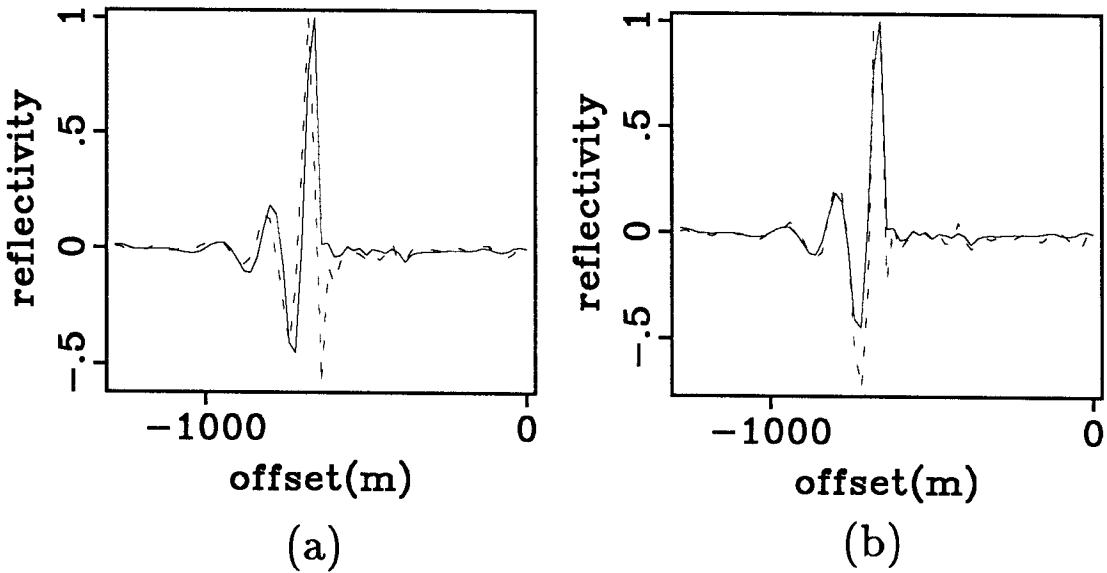
reflectivity

1

.5

0

-.5

-1000   0

offset(m)

(a)

reflectivity

1

.5

0

-.5

-1000   0

offset(m)

(b)

FIG. A.5. (a) Images at traveltime depth=.5 sec taken from Figure A.4. The solid curve is from Figure A.4a; the dashed curve is from Figure A.4b. Note the phase shift between the two curves. (b) The result of applying a $\pi/4$ phase shift to the dashed line in (a).

The differences between the two methods are not expected to produces big differences in the final migration result. Figure A.4 shows that the two methods give the same image except for a difference in the amplitude. Figure A.5 closely examines the images at a particular traveltime depth from Figure A.4. The figure shows the predicted phase shift. The amount of the phase shift is verified to be about $\pi/4$ by applying a $\pi/4$ phase shift to the dashed line.

The difference in the divergence correction and the phase shift between the two methods is the result of assuming a line source in the double-downward continuation method and a point source in the hybrid method. As noted earlier, line receivers were assumed in both methods. This means that a divergence correction and a phase shift should also be applied to the upgoing field if we want to use point receivers.